Journal of Sound and Vibration (1999) **221**(3), 505–524
Article No. jsvi.1998.2029, available online at http://www.idealibrary.com on IDEAL

EXPERIMENTAL INVESTIGATION OF NOISE REDUCTION IN SUPERSONIC JETS DUE TO JET ROTATION

R. NEEMEH, S. ALGATTUS AND L. NEEMEH
Department of Mechanical Engineering, Concordia University, 1455 *DeMaisonneuve Blvd. West, Montreal, Quebec, Canada H3G 1M8*

(*Received* 8 *June* 1998, *and in final form* 2 *November* 1998)

In the present work a swirl chamber is employed to study the effect of fluid rotation on noise reduction in supersonic jets. Fluid rotation is attained by means of a vortex chamber in which four moveable slabs are inserted. Schlieren photography is employed to visualize the flow and shock structure associated with any degree of fluid rotation. Static and Pitot pressure measurements are used to obtain the velocity distribution in the swirl chamber. These measurements show that the fluid inside the chamber is irrotational and that choking of the nozzle takes place at different critical pressure ratios depending on the degree of the fluid rotation. The resulting gain in noise reduction was determined using sound pressure measurements. The results show that small flow rotation ($M_\phi = 0{\cdot}39$) weakens the internal shock strength, reduces the cell length and decreases the screech noise generated. Higher fluid rotation is found to have no additional effect on noise reduction in supersonic jets. A maximum noise reduction of 12 dB is found to take place in jets with $1{\cdot}18 < M_j < 1{\cdot}4$.

1. INTRODUCTION

Supersonic jet flow can be produced by either a converging or a converging–diverging nozzle. In the present work, a convergent nozzle is employed to produce an imperfectly expanded supersonic jet consisting of two principal noise components: turbulent mixing noise and shock associated noise. The latter can be either broadband or screech tone. Turbulent mixing noise is present in subsonic as well as supersonic jets. It is generated from the interaction between the large turbulent structures propagating downstream, and the surrounding atmosphere. Shock associated noise is believed to be a result of the interaction of the turbulent structures created at the nozzle exit plane with the internal shock created in each cell. The screech tone component of shock-associated noise is discrete in nature and consists of various harmonics generated by an acoustic feedback of the disturbances created at the nozzle lip. These harmonics propagate through the cell and are fed back to the nozzle lip from outside the

0022-460X/99/130505 + 20 $30.00/0

cell. Another disturbance is then created which in turn propagates downstream, and the cycle repeats.

Previous studies to suppress the shock-associated noise were directed towards screech tone repression, which was believed to cause structural damage if its amplitude increased beyond a certain level. Methods used include porous plug [1], inverted velocity profile coanular jets [2], tabs [3–5], and nozzle asymmetry [6]. Ahuja and Brown [7] demonstrated the importance of tabs in the suppression of the screech tone.

Subsonic and supersonic swirling jets have been investigated as early as 1973 [8] with the conclusion that swirling jets mix more rapidly than axial jets. The swirl component of the velocity is found to decay more rapidly than the axial component as the jet mixes with surrounding air. Swirl is found to reduce noise, shorten the cell length and may cause, in some cases, reversed flow of air in the core when increased in strength.

In 1993, Samimy [9] experimentally investigated the effect of a vortex generator in the form of small tabs at the nozzle exit thereby eliminating the screech tone and distorting the shock cell structure in the entire jet cross-section. Carpenter [10] employed a linearized theoretical approach for swirling supersonic flow as applied to shock associated noise. He estimated the wavelength of the first peak related to total sound radiated power and found that swirl has potential as a method for suppressing shock cell noise. For stronger swirl, there may be a small loss in the thrust (1·6% for noise reduction of 19%).

Recently, Yu and Chen [11] studied the swirling effect on axial jets by using a scale model of 1 cm in exit diameter. They injected various strengths of swirl in the path of axial flow to induce it and analyzed the formation of the shock cell structure qualitatively. Their results indicated that swirl did not alter the quasi-periodic cell structure and that whether or not the jet is swirling, the screech tones are present due to shock cell existence. Furthermore, no consistent trend was found regarding noise reduction with increasing swirl in the flow. This can be explained by the fact that the injected tangential swirl does not have enough inertia to drag the axial jet to swirl.

The primary objective of the present work is to experimentally determine the effect of swirling flow on jet noise suppression using a small-scale, 10-mm inside diameter nozzle. The swirling chamber, which allows variation in the swirl velocity for any given jet pressure ratio without any additional disturbances, will be introduced in the following section. This method of noise suppression will be investigated visually using Schlieren photography, acoustically using a signal frequency analyzer and by means of detailed static and pitot pressure measurements carried out in the vortex chamber.

2. EXPERIMENTAL APPARATUS AND PROCEDURES

The experimental apparatus consists of a vortex chamber to generate a swirl flow of different magnitudes (strength). The chamber has a diameter of 254 mm, a height of 38 mm and is capable of producing swirling flow with variable

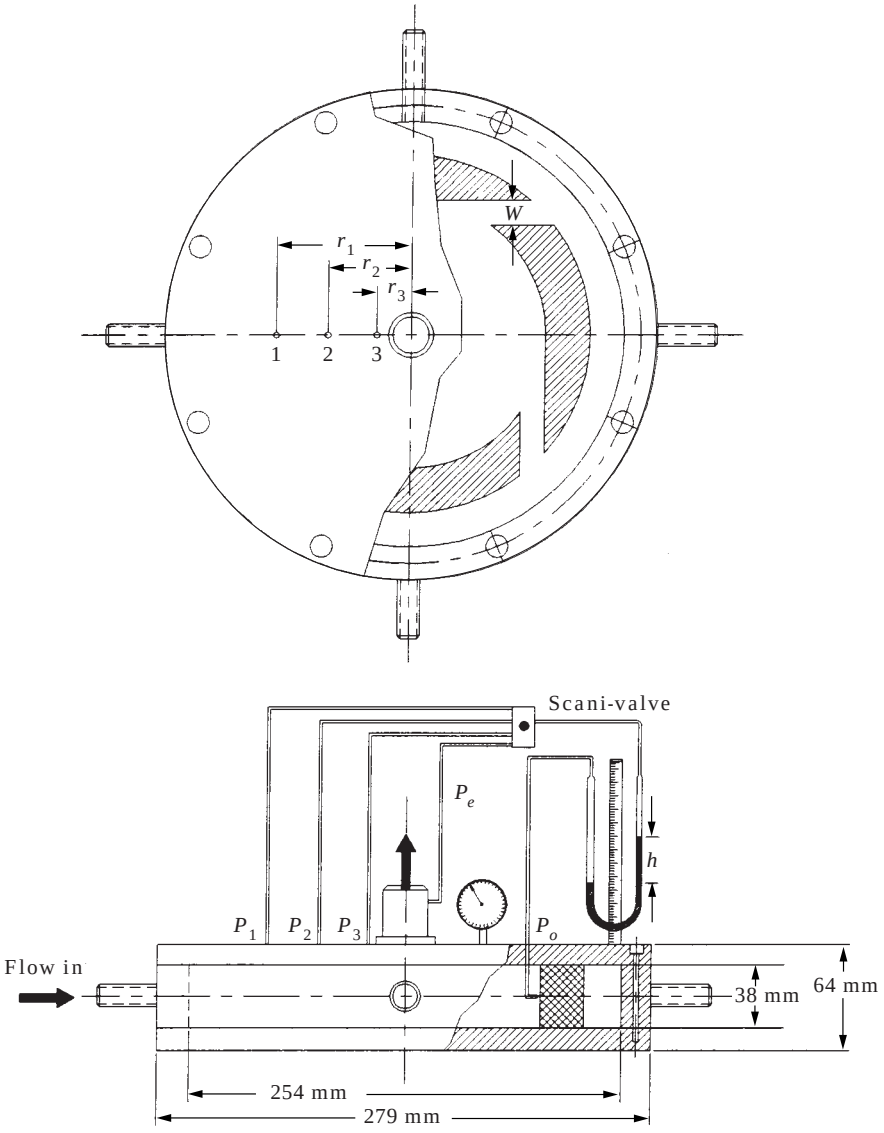

Figure 1. The vortex chamber apparatus.

intensity by using four movable slabs that are internally assembled to provide the circulatory motion (see Figure 1). The slabs have different settings in order to be able to change the magnitude of the swirl to the desired value and can also be removed to produce a jet without flow rotation. The air at normal conditions is temporarily stored in a large reservoir connected to the testing facility via four identical high pressure rubber hoses of 13 mm internal diameter and having a total area of 506 mm^2, which is four times greater than the nozzle exit area. This condition insures that the nozzle always chokes before the inlets for all operating pressures. The supply pressure and the mass flow rate to the plenum chamber are controlled by means of a pressure regulating valve.

For static pressure measurements, three pressure taps were drilled along the radial direction. These pressure taps are 2 mm in diameter. This diameter was carefully chosen to avoid any disturbances to the flow and yield accurate readings. The static pressure taps were located at radial locations $r_1 = 75$ mm, $r_2 = 53$ mm and $r_3 = 36$ mm corresponding to static pressures P_1, P_2, and P_3 respectively. In addition to the static pressure taps, a Pitot tube was inserted in the chamber to read the total pressure of the flow entering the chamber from the four ports. The pitot and static pressure readings were used to determine the flow velocities at the three radii mentioned above.

A schematic of the Schlieren system used in the present work is shown in Figure 2. It consists of two parabolic mirrors, 1230 mm in focal length. The light source is a 2-kV spark with a duration time of less than 1 μs. The light source is located in front of the condenser lenses. These lenses and the first knife edge are used to obtain a light source, 1 mm^2 in area. The knife edge was positioned at the focal point of the first parabolic mirror to yield parallel light beams, which pass through the test section. The light rays then reflect from the second parabolic mirror and converge at the focal point where another knife edge is used to cut part of the light, producing the Schlieren effect on the image of the test section where a camera is placed. An open shutter camera is used to take the instantaneous photograph. A continuous video camera was also employed to determine the behavior of the flow in the jet as well as the flow exit angle at the nozzle exit plane.

The acoustical results were determined using a signal frequency analyzer. The microphone is first calibrated using the calibration instrument such that it records 94 dB at a frequency of 1 kHz when the instrument is operated. The

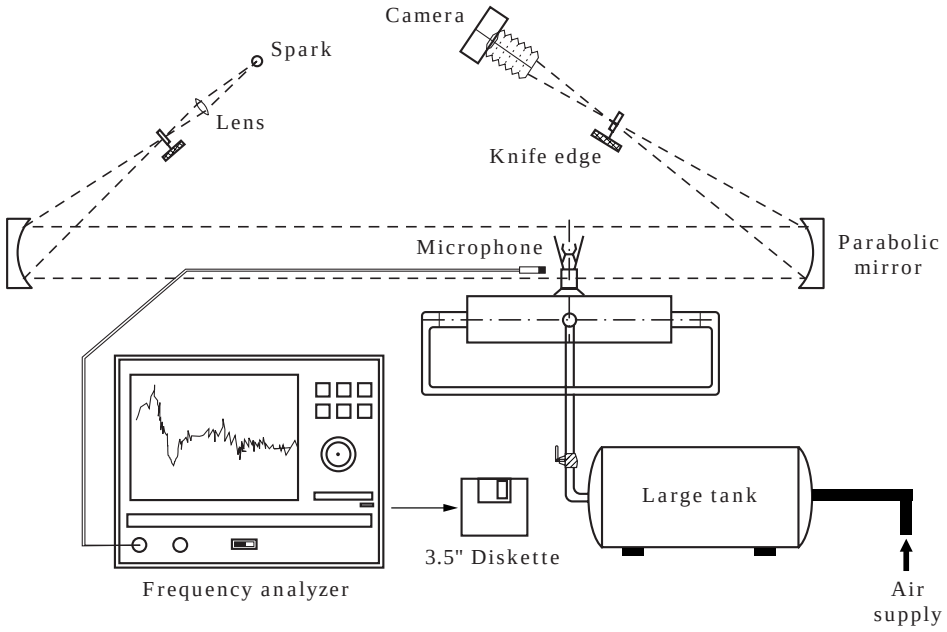

Figure 2. Experimental set-up of optical and acoustical equipment.

condenser microphone is then aligned with the nozzle exit plane at a distance equal to half the inside diameter of the nozzle and connected to a signal frequency analyzer (B&K 2035) equipped with a scan screen to display the signals. The operating valve is then opened to allow air from a pressure reservoir into the settling chamber to cover a wide range of stagnation pressures. The pressure of the settling chamber is monitored from a gauge connected to it. The microphone is isolated from all vibrating objects to ensure the reading is that of the nozzle noise only. The output data is stored in ASCII delimited format to be analyzed using any spread sheet software (in this study MS Excel, is used).

3. EXPERIMENTAL RESULTS AND DISCUSSION

Supersonic jets were produced using the vortex chamber apparatus described in the previous section. Moving radially, the four slabs inside the chamber varied the tangential component of the fluid velocity of the jet. Initially, the fluid emanates from four slots with a relatively low velocity. The fluid then accelerates to higher velocities as it approaches the nozzle exit. The results obtained from the detailed pressure and velocity measurements are presented in the next section followed by those from the schlieren photography and acoustic noise measurements.

3.1. PRESSURE AND TANGENTIAL VELOCITY MEASUREMENTS IN THE VORTEX CHAMBER

The total pressure of the flow, P_o, entering the swirl chamber, was measured by means of a Pitot tube placed at one of the four slots exit plane. The static pressures P_1, P_2 and P_3 were measured from the three static taps located at the three radial locations mentioned above. From the total and static pressure measurements, the velocity of the jet exiting the slots and those at the two smaller radii were calculated from the relation

$$v = \sqrt{2(P_o - P)/\rho},$$

where V is the fluid velocity, P_o is the total pressure, P is the static pressure and ρ is the fluid density. The results for a jet total pressure ranging between 10 and 250 kPag and for three different slot sizes of 16, 13 and 9·5 mm, respectively, are presented in Figure 3. As noted in the figure, using a larger slot size (16 mm) produces a weaker velocity than the use of a smaller slot size (9·5 mm). The jet velocity is also found to increase monotonically with the jet total pressure until the choking condition is reached. With fluid rotation, choking of the jet does not take place at the same value of P/P_o as that measured in jets without rotation. To find the exact pressure where choking takes place, another pressure tap was inserted near the nozzle exit plane, as shown in Figure 1. The static pressure at the nozzle exit was measured for every jet total pressure for the three jet rotation cases mentioned above. The results are presented in Figure 4. To determine the jet total pressure at which choking takes place, another graph was plotted for the exit pressure, P_r, normalized to the jet total pressure, P_o, versus the jet total pressure. As noted in Figure 5, the ratio of the static to total pressure gradually

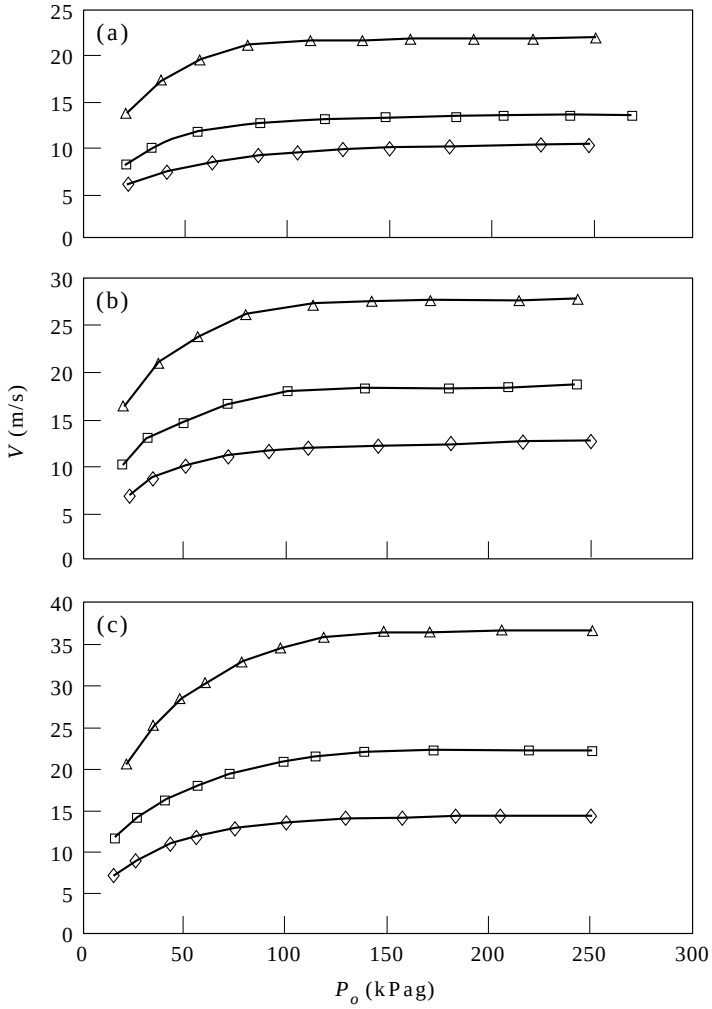

Figure 3. Fluid velocity versus jet total pressure for various slot sizes., (a) slot size = 16 mm; (b) slot size = 13 mm; (c) slot size = 9·5 mm; ◇, V_1; □, V_2; △, V_3.

decreases to reach a constant value at which point the choking condition has been reached. This critical pressure ratio is found to decrease with the decrease in the slot size or the increase in the degree of initial jet tangential velocity introduced to the flow. To analyze these results one has to first understand the nature of the flow emanating from the four slots and how it varies with the chamber radius. At large radii, the flow velocity is small and can therefore be analyzed using incompressible 2-D) Navier–Stokes equations. These equations indicate that the flow is irrotational (Γ = constant) and that

$$V_1 \cdot r_1 = V_2 \cdot r_2 = V_3 \cdot r_3.$$

This relation was verified for the three cases rotation by presenting $V*r$, normalized to r_1, for taps 2 and 3. The results are presented in Figure 6. From these results, it can be concluded that the fluid inside the chamber behaves as an irrotational vortex as it approaches the nozzle inlet.

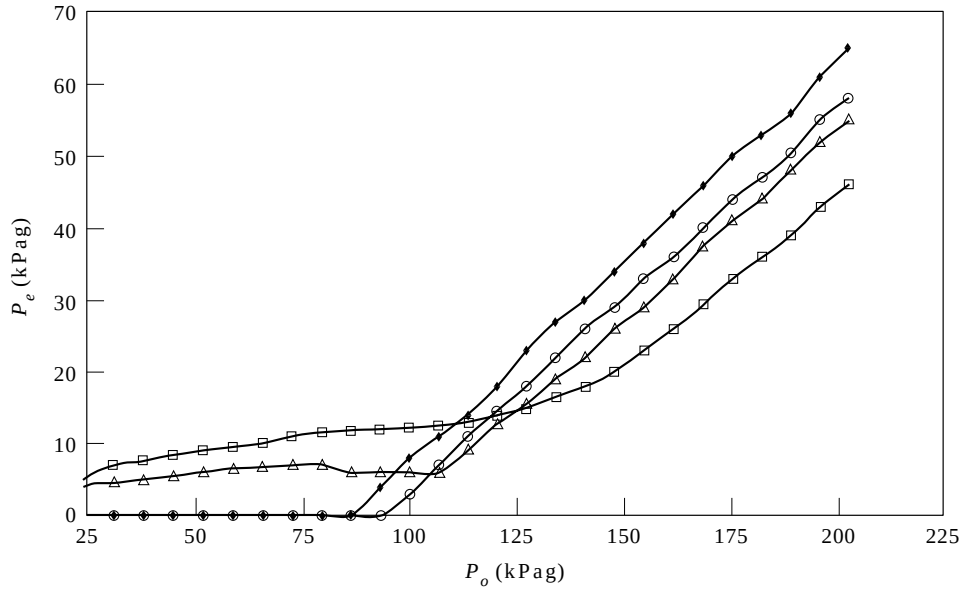

Figure 4. Static pressure at nozzle exit versus jet total pressure; ◆, no swirl; ○, slot size = 16 mm; △, slot size = 13 mm; □, slot size = 9·5 mm.

3.2. SWIRL MACH NUMBER AT NOZZLE EXIT

The fluid enters the nozzle with irrotational flow conditions, then propagates in a constant area tube before exiting to the atmosphere. Without fluid rotation inside the cylindrical chamber, and assuming frictionless flow, the fluid exiting

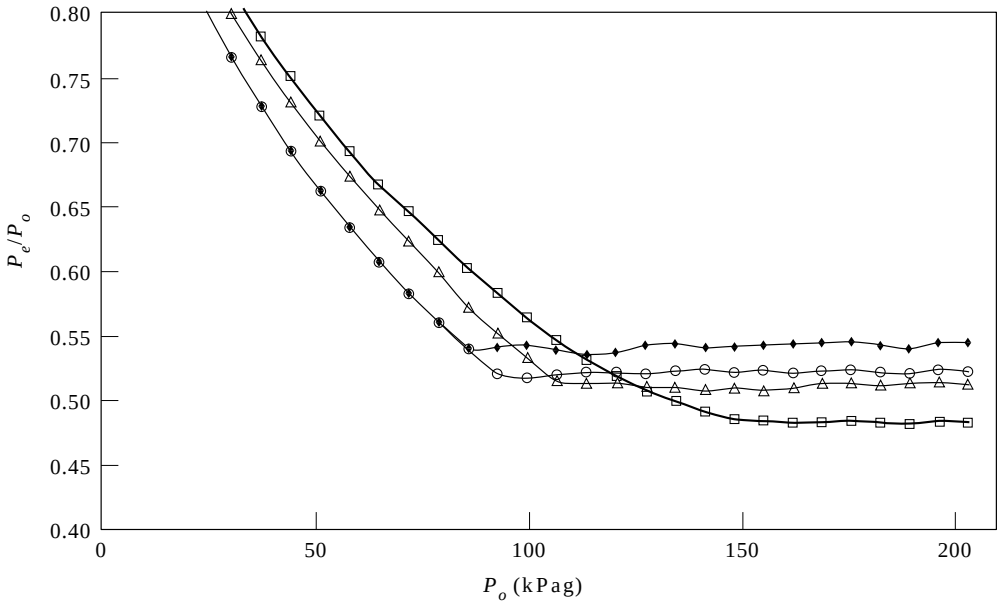

Figure 5. Static to total pressure ratio at nozzle exit versus jet total pressure; ◆, no swirl; ○, slot size 16 mm; △, slot size = 13 mm; □, slot size = 9·5 mm.

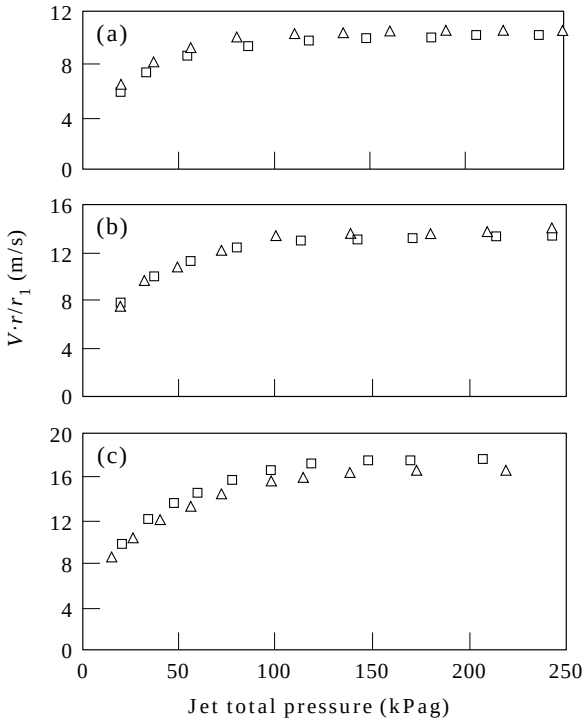

Figure 6. Experimental verification of fluid irrotationality inside the vortex chamber; (a) low swirl; (b) medium swirl; (c) high swirl. □, Experimental, $r/r_1 = 0{\cdot}48$; △, experimental, $r/r_1 = 0{\cdot}75$.

the nozzle is uniform. With fluid rotation, one may assume that swirl is being imposed on the flow exiting the nozzle and the tangential component of the velocity behaves in a similar fashion as that shown in Figure 7. The tangential component of the velocity was determined indirectly using Schlieren photographs of the flow at the nozzle exit plane. A very light nylon string was placed at the nozzle lip. Without fluid rotation the string takes the axial direction. With fluid rotation, the string takes the flow direction, which makes an angle θ the nozzle axis. The ratio of the tangential velocity to the axial velocity is equal to

$$V_\theta / Va = M_\theta / Ma = \tan(\theta)$$

and the total Mach number M is equal to

$$M^2 = M_a^2 + M_\theta^2,$$

where M_a and M_θ are the axial and the tangential Mach numbers, respectively. The swirl Mach number, M_ϕ, is defined as

$$M_\phi = V_\theta / c_c,$$

where c_c is the critical sound speed.

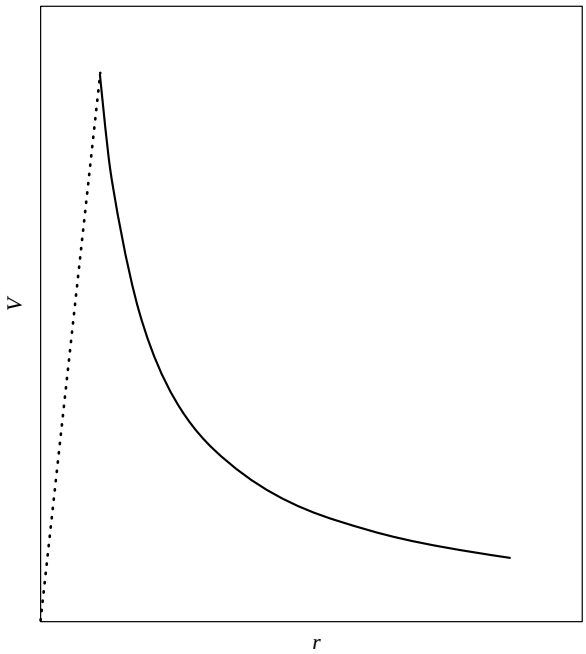

Figure 7. Typical tangential velocity distribution in a confined vortex flow; ---, vortex core, V = constant $*r$; —, V = constant/r.

Assuming isentropic conditions, the total Mach number was calculated from the ratio of the static pressure, measured at the nozzle exit, to the jet total pressure measured at the cylindrical chamber inlet. Using the value of θ, measured from the Schlieren photographs, the two components of the Mach numbers are then

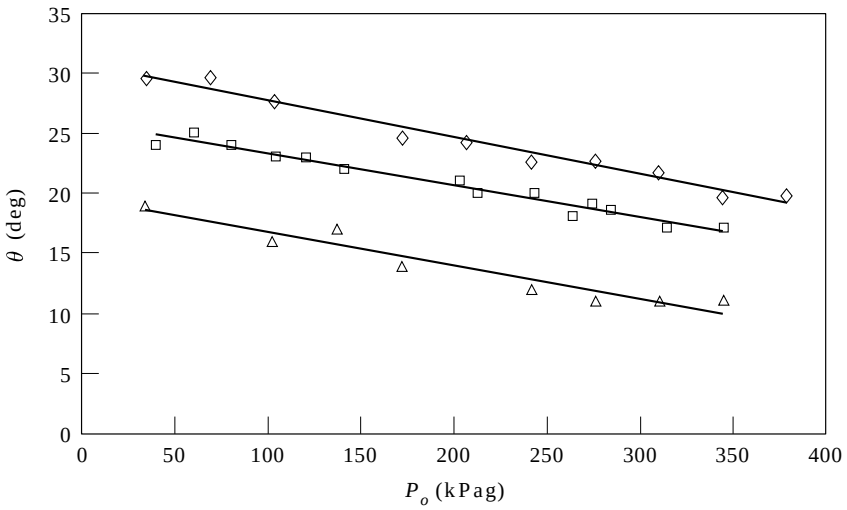

Figure 8. Flow angle with the nozzle axis at the nozzle exit: △, slot size = 16 mm; □, slot size = 13 mm; ◇, slot size = 9·5 mm.

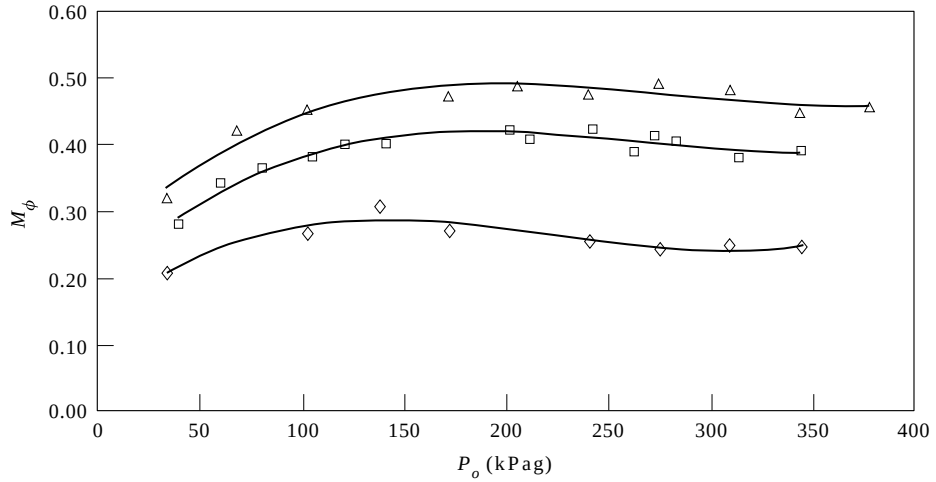

Figure 9. Calculated values of the tangential velocity at the nozzle exit versus jet total pressure for different slot sizes; ◇, slot size = 16 mm; □, slot size = 13 mm; △, slot size = 9·5 mm.

determined. The axial and tangential components of the fluid velocity are obtained by multiplying the Mach number by the local sound speed, c, where

$$c = (p_e/P_o)^{\gamma-1/2\gamma} c_o$$

and c_o is the sound speed of the air supply, and γ is the specific heat ratio.

For the three cases tested, the measured angles of the flow are as shown in Figure 8. The calculated values of the swirl Mach number are shown in Figure 9. As noted in the figure, the swirl Mach number, M_ϕ, increases with the increase

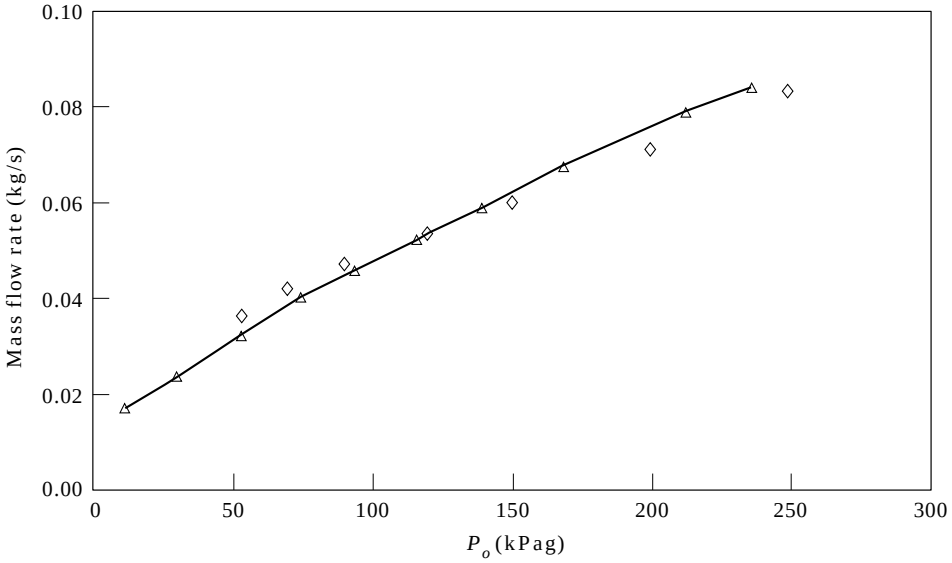

Figure 10. Mass flow rate versus jet total pressure for the 16-mm slot size △, experimental mass flow rate; ◇, theoretical mass flow rate.

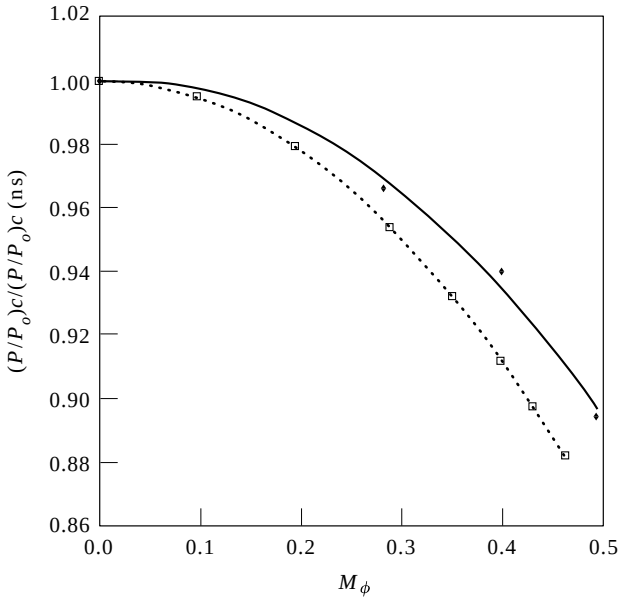

Figure 11. Critical pressure ratio with swirl normalized to that without swirl versus the swirl Mach number: ◆, experiment; □, theory.

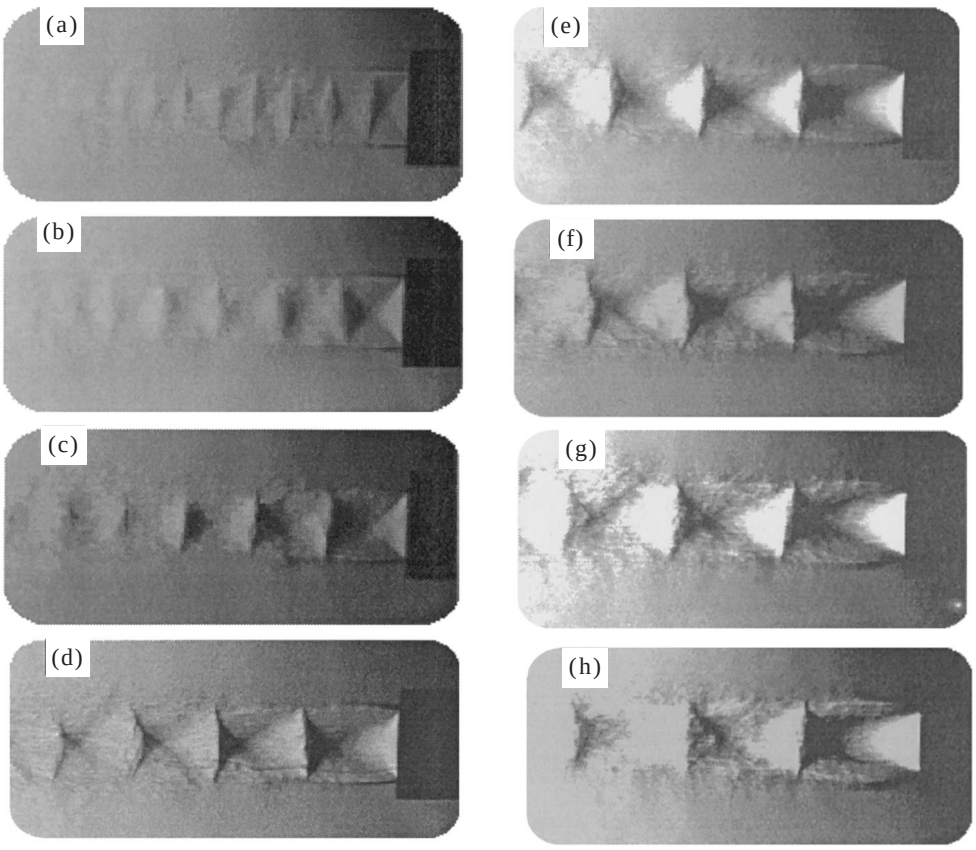

Figure 12. Schlieren photographs of supersonic jets without swirl: (a) $M_j = 1{\cdot}05$; (b) $M_j = 1{\cdot}18$; (c) $M_j = 1{\cdot}28$; (d) $M_j = 1{\cdot}37$; (e) $M_j = 1{\cdot}44$; (f) $M_j = 1{\cdot}51$; (g) $M_j = 1{\cdot}57$; (h) $M_j = 1{\cdot}62$.

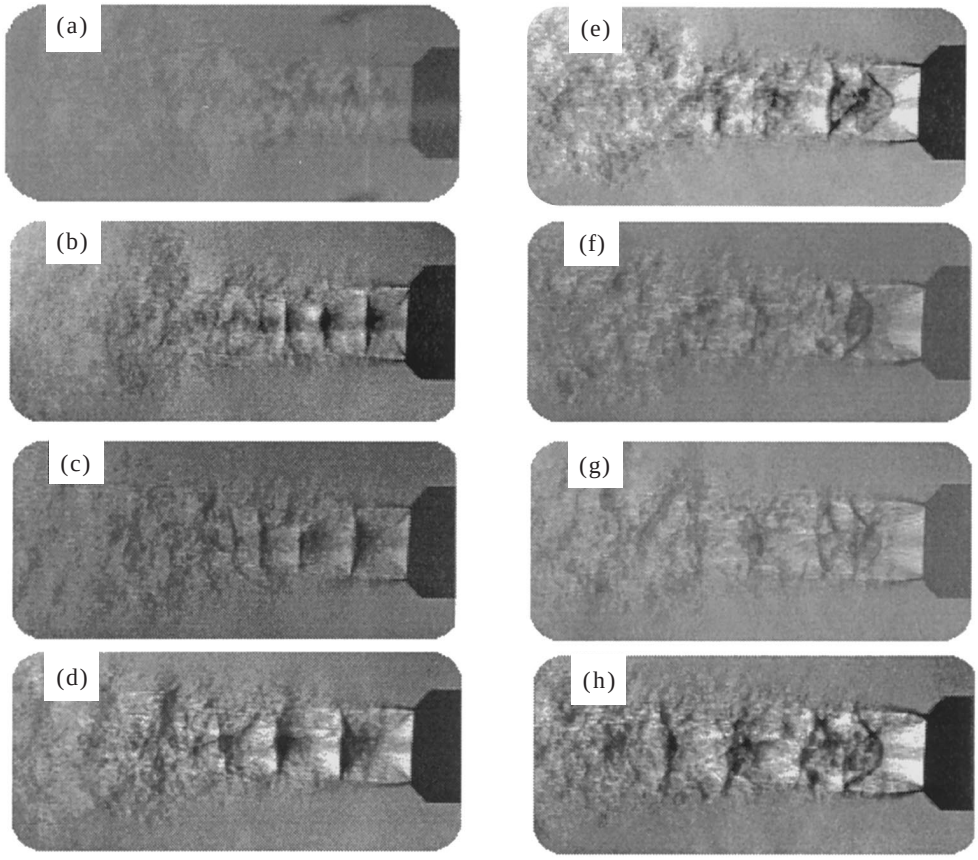

Figure 13. Schlieren photographs of supersonic jets with low swirl: $M_j = 1{\cdot}05$; (b) $M_j = 1{\cdot}18$; (c) $M_j = 1{\cdot}28$; (d) $M_j = 1{\cdot}37$; (e) $M_j = 1{\cdot}44$; (f) $M_j = 1{\cdot}51$; (g) $M_j = 1{\cdot}57$; (h) $M_j = 1{\cdot}62$.

in the jet pressure until it reaches a maximum value after which it remains constant. The figure also shows that for any given jet pressure, M_ϕ increases with the decrease in the slot exit area. The mass flow rate was calculated based on the axial component of the velocity and was compared with the measured inlet mass flow rate into the cylindrical chamber. The results are shown in Figure 10, for the 16-mm case. Excellent agreement was noted between the experimental values and the theoretical one indicating the validity of our assumption that the circulatory flow is superimposed on the main uniform flow. To further verify our assumption, a theoretical value of the critical pressure ratio was calculated and compared with the experimental values presented in Figure 5. The critical pressure ratio was calculated based on the axial Mach number being unity and the swirl Mach number is as given in Figure 9. The results are presented in Figure 11. As seen in the figure, the theoretical results are in fair agreement with the experimental ones and the critical pressure ratio is dependent on the degree of the initial swirl. A higher swirl results in a lower critical pressure ratio.

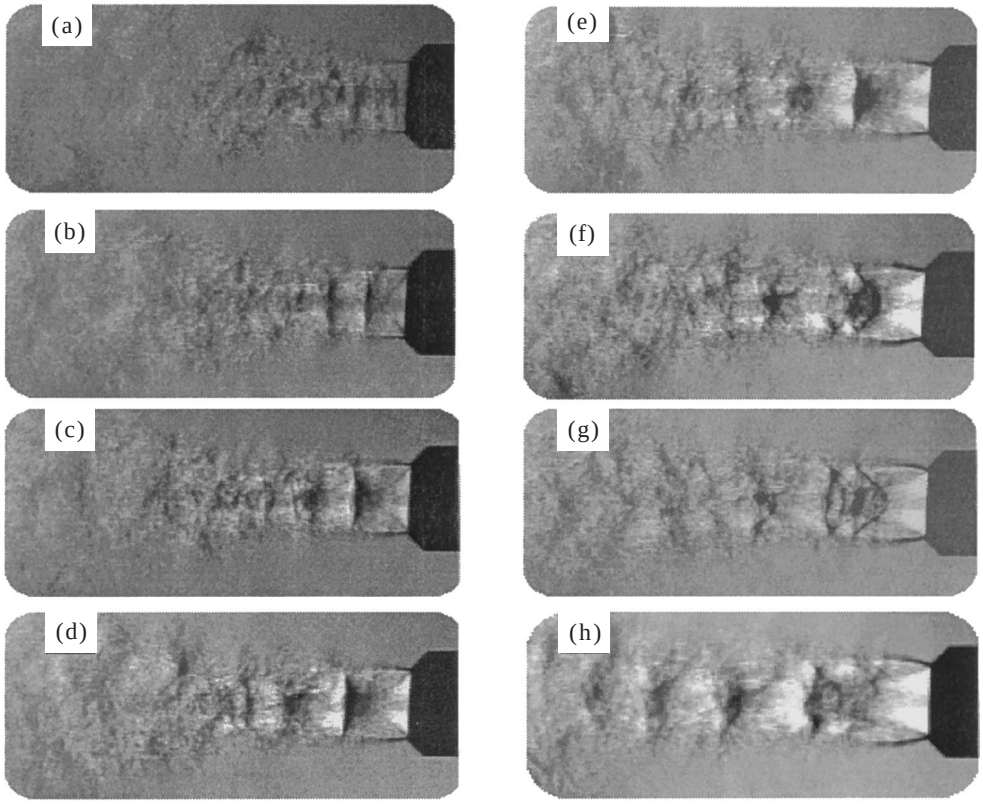

Figure 14. Schlieren photographs of supersonic jets with medium swirl: (a) $M_j = 1{\cdot}05$; (b) $M_j = 1{\cdot}18$; (c) $M_j = 1{\cdot}28$; (d) $M_j = 1{\cdot}37$; (e) $M_j = 1{\cdot}44$; (f) $M_j = 1{\cdot}51$; (g) $M_j = 1{\cdot}57$; (h) $M_j = 1{\cdot}62$.

3.3. EFFECT OF SWIRL ON SHOCK CELL STRUCTURE

Separate tests were run for various jet Mach numbers, M_j, for optical and acoustical measurements. Optical tests were carried out to examine the jet structure. The jet exhausts to the atmospheric pressure, P_a. The jet Mach number is calculated using the following isentropic relation:

$$M_j = \left[\frac{2}{\gamma - 1}\left[\left(\frac{P_c}{P_a}\right)^{\gamma - 1/\gamma} - 1\right]\right]^{1/2},$$

where γ is the specific heat ratio for air.

A sample of the Schlieren photographs taken are presented in Figures 12–15 for four cases: jets without swirl, jets with low swirl (16-mm slot size), jets with medium swirl (13-mm slot size) and jets with high swirl (9·5-mm slot size), respectively. As seen in the figures, a stronger swirl results in a shorter cell length and jet Mach numbers higher than 1·37 result in secondary internal shock formation. The cell length and the position of the secondary shocks were measured from these photographs and the results are shown in Figure 16. The

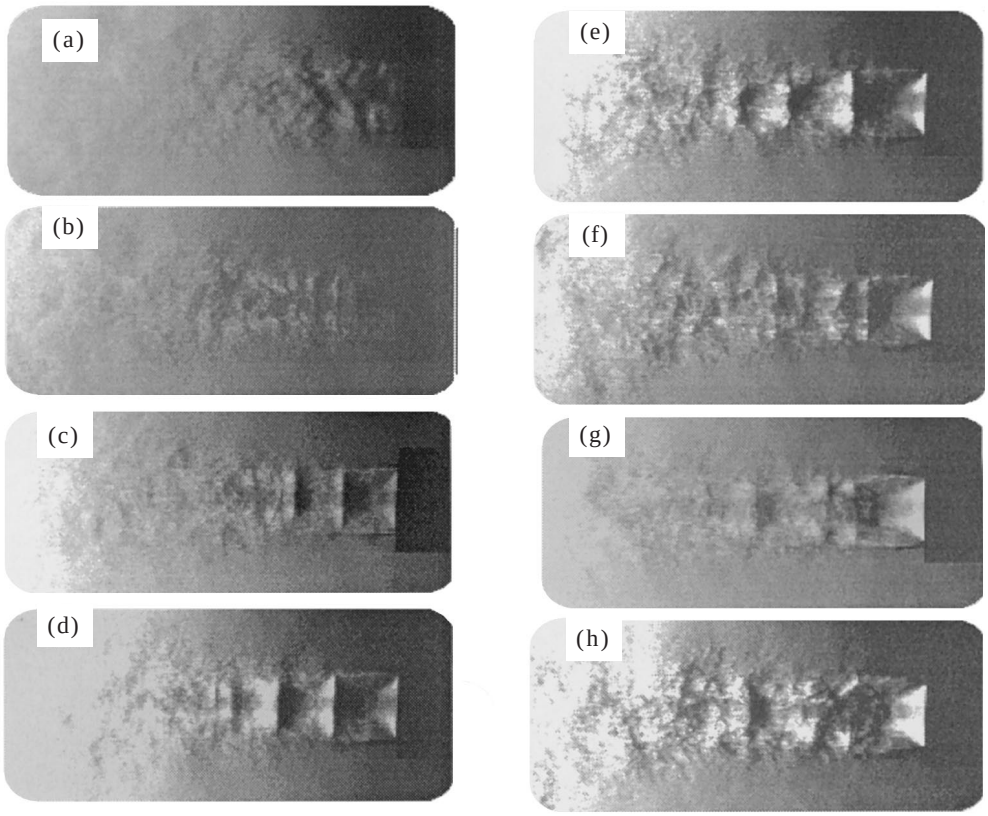

Figure 15. Schlieren photographs of supersonic jets with high swirl: (a) $M_j = 1{\cdot}05$; (b) $M_j = 1{\cdot}18$; (c) $M_j = 1{\cdot}28$; (d) $M_j = 1{\cdot}37$; (e) $M_j = 1{\cdot}44$; (f) $M_j = 1{\cdot}51$; (g) $M_j = 1{\cdot}57$; (h) $M_j = 1{\cdot}62$.

effect of swirl on jet growth is shown in Figure 17, for a jet Mach number of 1·37. As noted in the figure, swirl increases the spreading rate. With low swirl, and at an x/D ratio of 3, the jet spreads approximately 2·8 times that without swirl. High swirl is found to double the spreading rate.

The jet boundary of the inviscid core was measured from the Schlieren photographs. Great care was taken in these measurements to minimize the errors. The photographs were first magnified digitally to about 30 times their actual size, then projected onto a screen for measurements. The results are presented in Figure 18 for two discrete values of M_j, 1·28 and 1·57. Since swirl requires higher jet pressures to choke the flow, the effect of under-expansion is found to be less noticeable in jets with swirl than jets without swirl for the same jet total pressures. In the low swirl case, at $M_j = 1{\cdot}28$, the jet boundary exhibited a 3% diameter increase as opposed to an 8% increase in jets without swirl. Swirl is also found to decrease the degree of lateral flow expansion which is found to weaken the internal shock strength and the noise associated with it. This phenomenon will be demonstrated in the acoustic measurements of the next section.

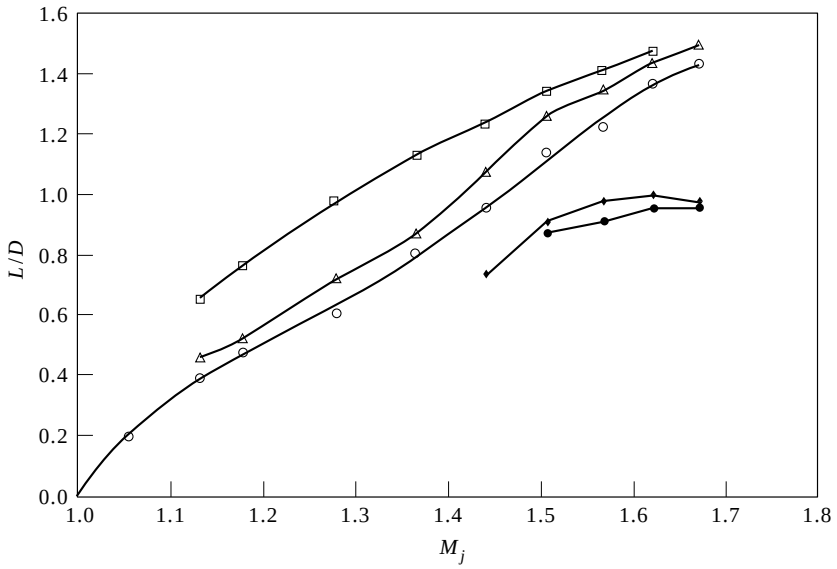

Figure 16. Cell length and secondary shock position versus M_j with and without swirl: □, no swirl; △, primary cell length, low swirl; ○, primary cell length, medium swirl; ◆, secondary shock position, low swirl; ●, secondary shock position, medium swirl.

3.4. ACOUSTIC RESULTS

A series of tests were run repeatedly for each configuration in order to insure the accuracy of the results. A sample of the obtained results of the narrow band spectra is presented in Figure 19 for jets with and without swirl at jet Mach numbers M_j of 1·18, 1·28, 1·37 and 1·44. As seen in the figure, the screech tones without swirl exhibit marked peaks. These peaks represent the sound pressure levels, SPL, which are greater than 130 dB. With low swirl (16-mm slot size), the

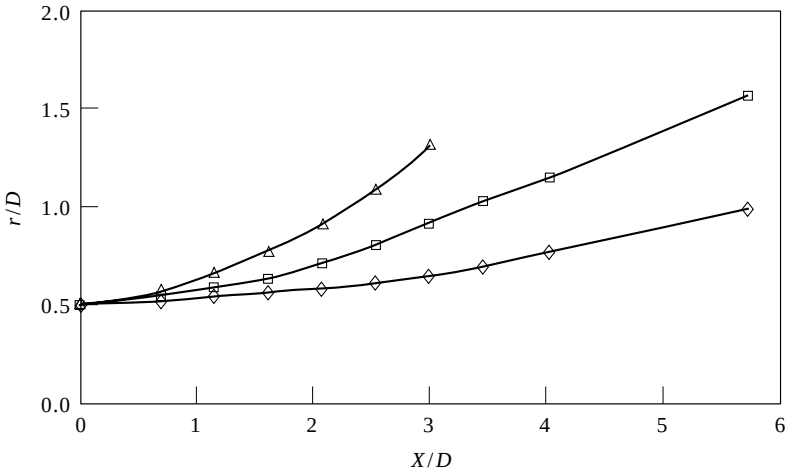

Figure 17. Growth of a circular jet with downstream distance: ◇, no swirl; □, low swirl; △, high swirl.

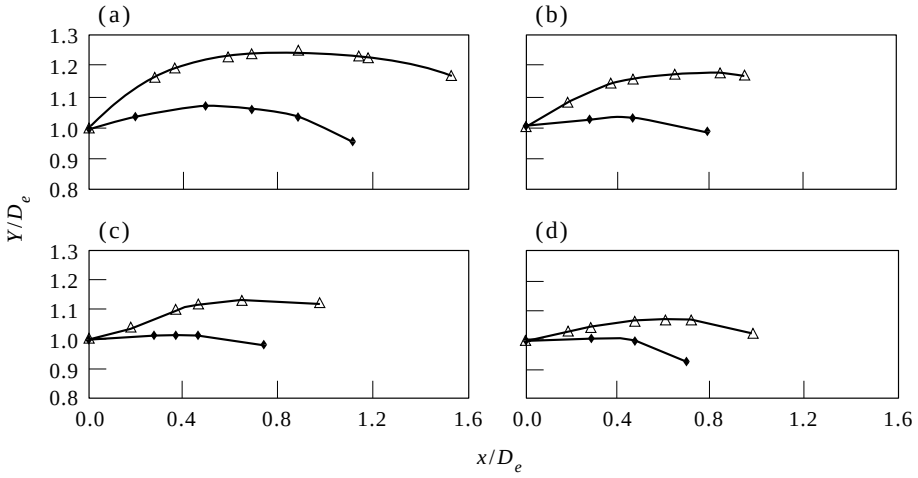

Figure 18. Jet boundary with and without swirl: (a) no swirl; (b) low swirl; (c) medium swirl; (d) high swirl. ◆, $M_j = 1{\cdot}28$; △, $M_j = 1{\cdot}57$.

screech tone is suppressed and only the turbulent noise is observed. For high swirl (9·5-mm slot size) little improvement is noted in the sound pressure level. The maximum SPL, recorded for a wider range of jet pressures is shown in Figure 20. At low pressures and subsonic jet Mach numbers, swirl is found to yield higher SPL, values due to the better mixing ability of the jet fluid with the surrounding ambient air. This increases the turbulence level and the sound level associated with it. At a jet Mach number greater or equal to 1·18, swirl is found to suppress screech noise thus reducing the maximum SPL, by as much as 15 dB

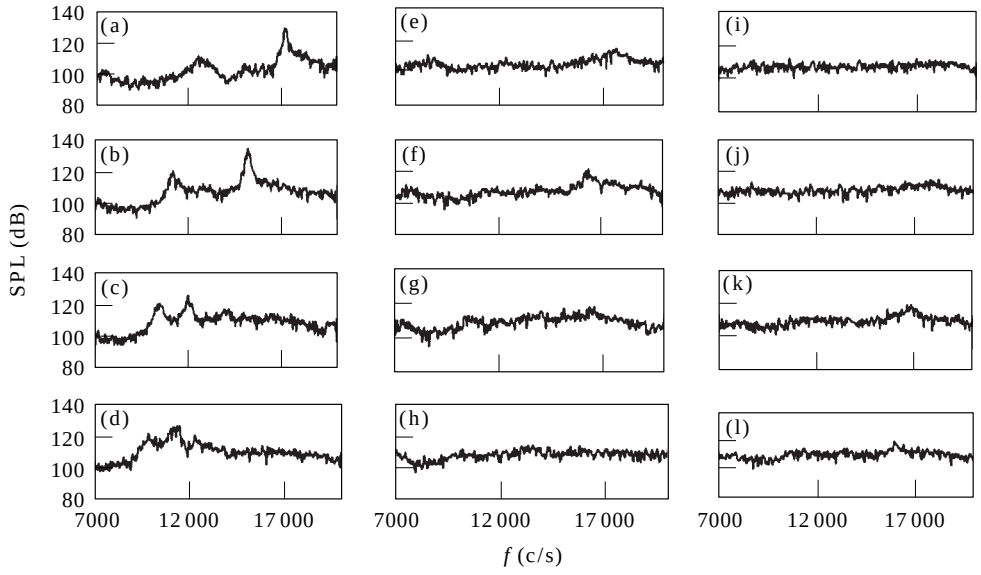

Figure 19. Typical narrow band spectra with and without swirl. No swirl: (a) $M_j = 1{\cdot}18$; (b) $M_j = 1{\cdot}28$; (c) $M_j = 1{\cdot}37$; (d) M_j 1·44. Low swirl: (e) $M_j = 1{\cdot}18$; (f) $M_j = 1{\cdot}28$; (g) $M_j = 1{\cdot}37$; (h) $M_j = 1{\cdot}44$. High swirl: (i) $M_j = 1{\cdot}18$; (j) $M_j = 1{\cdot}28$; (k) $M_j = 1{\cdot}37$; (l) $M_j = 1{\cdot}44$.

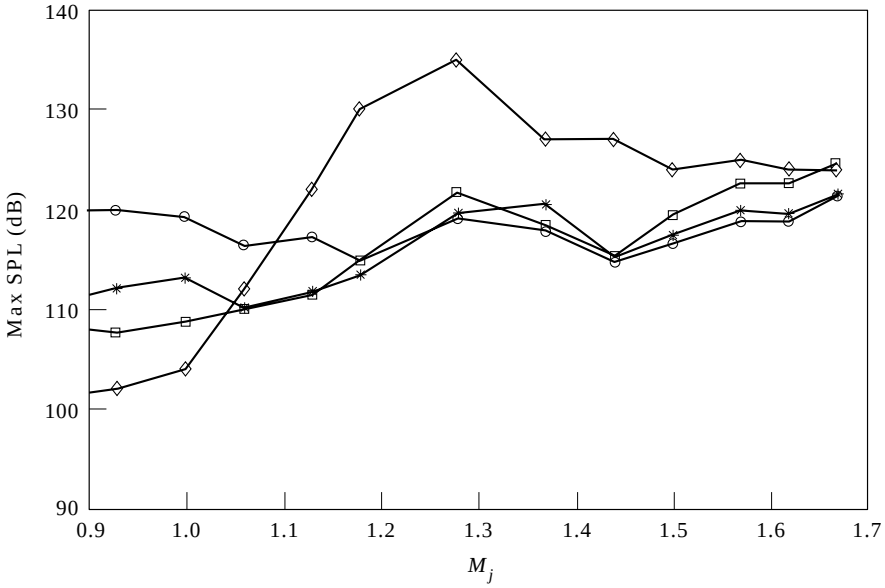

Figure 20. SPL versus M_j with and without swirl: ◇, no swirl; □, low swirl; ∗, medium swirl; ○, high swirl.

when compared to the no swirl case. The maximum effect is found within jet Mach numbers of 1·18 and 1·44. At jet Mach numbers higher than 1·44, the SPL difference decreases monotonically with the increase in jet pressures until no difference exists. This occurs at M_j greater than 1·68.

The resonant frequency of the screech tone is shown in Figure 21 together with the maximum SPL, associated with it. As noted in the figure, swirl results in a considerable decrease in the maximum value of the SPL while slightly increasing the frequency and the Strouhal number. The latter effect is expected due to the decrease in the shock cell length with magnitude of the swirl.

The overall SPLs as a function of the angular position from the centerline of the jet were also measured. The microphone was set at an arc position equal to

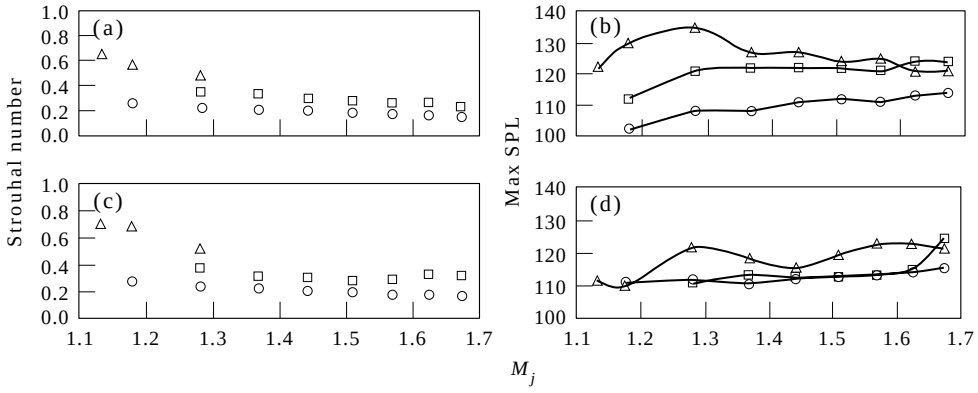

Figure 21. Strouhal number and SPL versus M_j with and without swirl: (a), (b) no swirl; (c), (d) low swirl. △, A; □, B; ○, C.

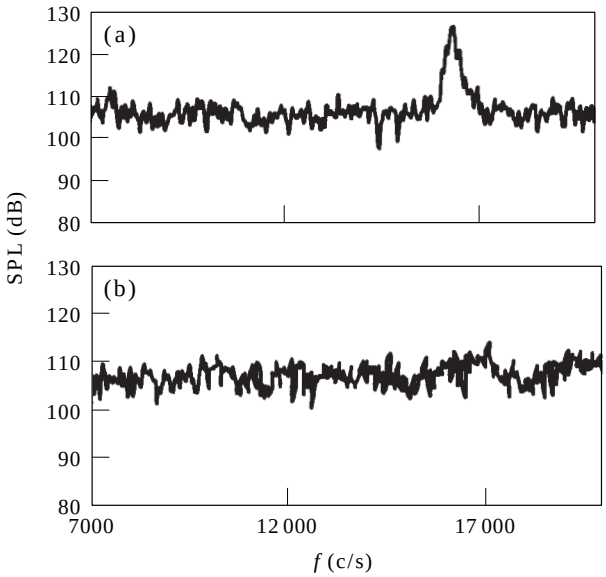

Figure 22. Noise spectra for a jet Mach number of 1·28 (30° from the centerline of exhaust nozzle): (a) no swirl; (b) low swirl.

20 nozzle diameters extending from the centerline of the nozzle exit. Measurements were carried out at 10° intervals until the surface of the swirl chamber was reached (∼100°). A sample of the noise spectra, measured at an angle of 30° is presented in Figure 22 for both a jet with low swirl and a jet without swirl. As noted in the figure, the major effect of swirl is in the screech noise component. With swirl, screech noise is practically eliminated. Similar results were obtained at all angles measured. The results are presented in

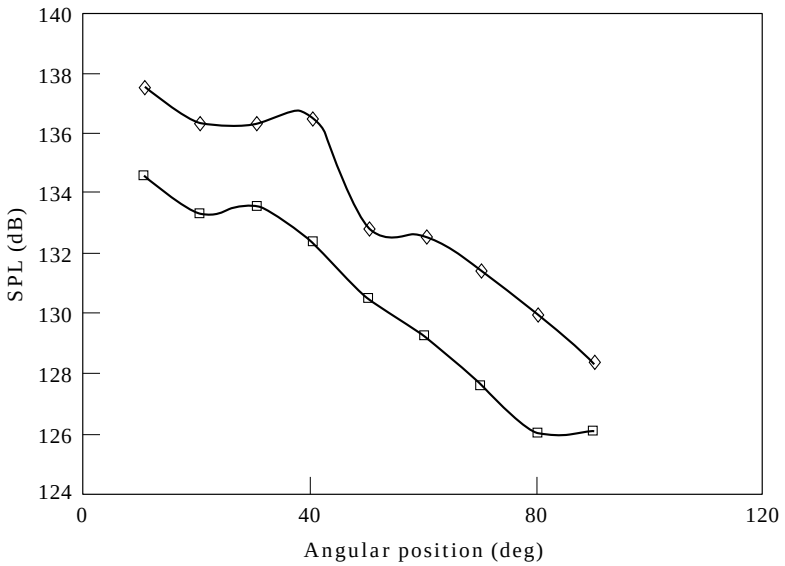

Figure 23. Overall SPLs as a function of angular position from jet axis: ◇, no swirl; □, low swirl.

Figure 23 for the overall sound pressure level as a function of the angular position. As noted in the figure, swirl decreases the overall sound pressure level by about 3·1 dB. The maximum pressure level, however, decreases by as much as 15 dB.

Swirl also results in a thrust loss when comparison is made for the same jet total pressure, or jet Mach number M_j. In the present work, the introduction of the swirl into the jet stems from the jet total pressure. An increase in the swirl magnitude is expected to decrease the jet axial component of the velocity and hence the mass flow rates exiting the nozzle. For the low swirl case, a 1·6% thrust loss is found to take place. With medium swirl the loss increases v dramatically to 6·5%.

Sound pressure measurements indicate that low swirl is as effective as high swirl as far as noise reduction is concerned. Combining this with the thrust loss results, the low swirl case is found to be the best alternative in terms of both noise reduction with minimal thrust loss.

4. CONCLUSION

The effect of swirl in noise reduction on supersonic jets was examined both optically, using Schlieren photography, and acoustically using a signal frequency analyzer. The results have shown that swirl behaves like an irrotational vortex as it approaches the nozzle. Using a large inlet area to the vortex chamber (slot size = 16 mm) resulted in a maximum value of the swirl Mach number, M_s, of 0·31 at the jet boundary. Decreasing the area was found to increase the swirl Mach number to a maximum measured value of 0·49.

The results obtained from the Schlieren photographs show that swirl does indeed affect the jet structure. As seen in the photographs, an increase in swirl yields a decrease in shock cell length, a decrease in the number of cells due to the increase in mixing with the surrounding fluid as well as the production of secondary shocks at higher pressures. Acoustically, for supersonic jets, low swirl is found to reduce the maximum SPL level as good as high swirl and by as much as 15 dB for M_j ranging between 1·18 and 1·4.

Swirl in supersonic jets was experimentally proven to reduce screech noise. However, in subsonic jets, it is better to use low swirl in order to minimize the turbulence effect resulting from the swirl.

REFERENCES

1. L. MAESTRELLO 1979 *AIAA Paper* 79-0673. An experimental study on porous plug jet noise suppression.
2. H. K. TANNA, C. K. W. TAM and W. H. BROWN 1981 *NASA CR*-3454. Shock associated noise reduction from inverted-velocity profile coanular jets.
3. L. BRADBURY and A. KHADEM 1975 *Journal of Fluid Mechanics* **70**, 801–813. The distortion of a jet by tabs.
4. H. K. TANNA 1977 *Journal of Sound and Vibration* **50**, 429–444. An experimental study of jet noise, part II: shock associated noise.
5. R. NEEMEH and A. ROSHANZAMIR 1994 *Proceedings of the* 3*rd International Congress on Air and Structure Born Sound and Vibration, Montreal, Canada*,

1177–1184. Experimental studies of single and twin supersonic jets noise and stability.
6. R. W. WLEZIEN and V. KIBENS 1986 *AIAA Paper* 86-0277. The influence of nozzle asymmetry on supersonic jets.
7. K. K. AHUJA and W. H. BROWN 1989 *AIAA Paper* 89-0994. Shear flow control by mechanical tabs.
8. R. SMITH 1973 *Aeronautical Quarterly* **24**, 167–178. An investigation of supersonic swirling jets.
9. M. SAMIMY 1993 *AIAA Journal* **13**, 609–619. Effect of tabs on the flow and noise field of an axisymmetric jet.
10. P. W. CARPENTER 1985 *A1AA Journal* **23**, 1902–1909. A linearized theory for swirling supersonic jets and its application to shock cell noise.
11. Y. YU and R.-H. CHEN 1997 *Journal of Sound and Vibration* **205,** 698–705. A study of screech tone noise of supersonic swirling jets.